The Unpredictable Bouncing Rotator: a Chaology Tutorial Machine

Michael Berry

H.H.Wills Physics Laboratory, Tyndall Avenue, Bristol BS8 1TL,U.K.

1. INTRODUCTION

For exploring and teaching the principles of nonlinear dynamics, or chaology [1], it is common to make use of mathematical models (e.g. discrete mappings), which are relatively easy to analyze but abstract, and also simple machines (e.g. a conical pendulum whose magnetic bob is deviated by several fixed magnets), whose motion can be readily observed but which are hard to analyze. Here I describe a way to retain the advantages of both: a machine that displays unpredictable behaviour and also inspires a series of mathematical models illustrating KAM tori, bifurcation of periodic orbits, Hamiltonian chaos, stable fixed points and strange attractors, leading eventually to the discovery of the source of the unpredictability, which turns out not to be obvious.

The machine, which I call 'the bouncer', is illustrated in Fig.1a. R is a rotator consisting of two light hollow balls containing magnets. Its axis A_1 swings to and fro at the top of a pendulum, pivoted at A_2, whose bob is the heavy driving ball D. The regular swinging of D is itself driven by an electromagnet, located in the base B and switched by a circuit that senses each approach of a magnet inside D. As well as rotating inertially and being swung by D, R occasionally bounces because its balls are repelled by a magnet M, situated just above A_2 on the pendulum. As a result of these in-

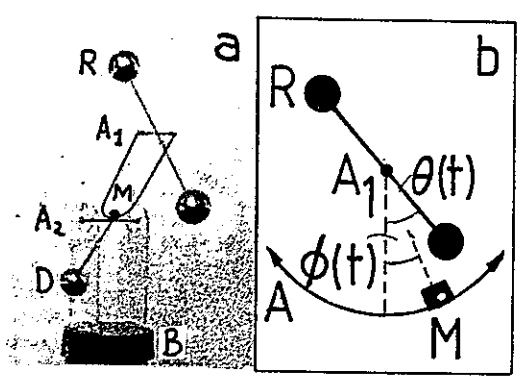

Fig.1 a) The bouncer; b) geometry and coordinates in frame where the axis A_1 is fixed.

fluences R rotates in an apparently irregular manner, clockwise and anticlockwise, on time scales from several seconds (the driving period) to several weeks (i.e. until the battery is exhausted).

The bouncer is manufactured in Taiwan, and sold in the U.K. as 'space ball' and in the U.S. as 'space trapeze'.

To model the system we move to the frame in which the axis A_1 is at rest (Fig.1b), and let the rotator's single degree of freedom be the angle $\theta(t)$ that it makes with the vertical. In this frame, M swings about A_1 on a circular arc with angle $\phi(t)$. Because D is heavy it is a sufficient approximation to consider its motion unaffected by that of R, so $\phi(t)$ is a periodic function, which we model as

$$\phi(t) = A \sin 2\pi t. \qquad (1)$$

By observation, the driver amplitude A is about 90^o. Equation (1) defines the unit of time as the driving period (actually about 1.85s). The phase space for R's motion has coordinate θ and (angular) momentum $p \equiv d\theta/dt$, with ranges $0 \leq \theta < \pi$ (except for the model of section 5) and $-\infty < p < +\infty$. Motion depends on the torques acting on R, and these will be specified in four increasingly sophisticated models. For each model the long-time behaviour of orbits will be displayed as discrete mappings on surfaces of section corresponding to integer times t (i.e. when the driving pendulum is vertical with ϕ increasing).

2. THE FIRST MODEL: NO DISSIPATION, COMPULSORY BOUNCING

To find the simplest model giving chaos we first assume, in flagrant disregard of observation, that M's repulsion is strong enough to cause R to bounce at every encounter, i.e. at times t_B such that

$$\theta(t_B) = \phi(t_B) \bmod \pi . \qquad (2)$$

These bounces are assumed elastic and so they reverse the relative angular velocity, thus relating momenta p_+ and p_- after and before a bounce by

$$p_+(t_B) = - p_-(t_B) + 2d\phi(t_B)/dt. \qquad (3)$$

Lack of dissipation implies that between bounces p is constant and θ changes linearly, i.e.

$$\theta(t) = \theta(t_B) + p_+(t_B)\,(t-t_B). \qquad (4)$$

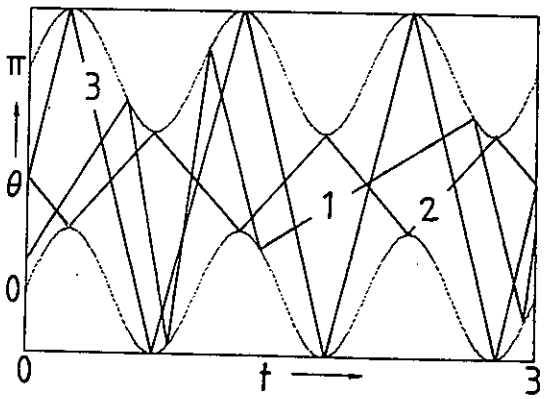

Fig.2 Orbits of first model with $A=50^o$ showing a typical orbit (1), an unstable 2-bounce periodic orbit (2), and a stable 2-bounce periodic orbit (3). The sinusoids are $\phi(t) \bmod \pi$

Motion according to these rules resembles that of the clapper in a swinging bell or, in terms of a recent theory of thermal conductivity [2], that of the one-body ding-a-ling model on a circle, with infinitely massive dongle. Some orbits are shown in Fig.2

An essential ingredient in studying the stability of orbits is the phase-space deviation matrix M between any two times t_1 and t_2 ; this is defined as

$$M \equiv \partial(\theta_1, p_1) / \partial(\theta_2, p_2) \tag{5}$$

Because friction has been neglected, detM=1 and the surface-of--section mapping is area-preserving. Between bounces, motion is integrable and hence neutrally stable, so we must study M for intervals which include a bounce time t_B; for such an interval an elementary calculation gives

$$\mathrm{Tr}M = -2(1+X) \tag{6}$$

where

$$X \equiv T\frac{d^2\phi(t_B)}{dt^2} = \frac{-(2\pi)^2 T\phi(t_B)}{\overline{p_-(t_B)-d\phi(t_B)}/dt \quad \overline{p_-(t_B)-d\phi(t_B)}/dt} \tag{7}$$

with $T \equiv t_2 - t_1$ and where (1) has been used.

The bounce is locally stable if and only if the eigenvectors of M lie on the unit circle, i.e. if $|\mathrm{Tr}M| < 2$, or $-2<X<0$. It follows that bounces from outside (opposite signs for $d^2\phi/dt^2$ and $\theta-\phi$ near the bounce) are always locally unstable, and so periodic orbits made up of sequences of such bounces (e.g. 2 in Fig.2) are globally unstable. Outside bounces therefore constitute a source of chaos. On the other hand, the stability of bounces from inside (i.e. the same signs for $d^2\phi/dt^2$ and $\theta-\phi$ near the bounce) depends on circumstances.

To study this, consider the simplest periodic orbit consisting of bounces from inside (3 in Fig.2). This has two bounces and period 1 and corresponds to a fixed point on the surface of section, with

$$\theta = \pi/2 \ , \ p = 2(\pi+2A) \tag{8}$$

Its total bounce matrix M_2 has

$$\mathrm{Tr}M_2 = 2+4X(X+2) \tag{9}$$

and (7) with T=1/2 gives X as

$$X = -\pi^2 A/(\pi+2A). \tag{10}$$

It follows that the orbit is stable if $0<A<A_{cr}$ where $A_{cr} = 2\pi/(\pi^2-4) = 1.07 = 61.33^\circ$ (with marginal stability for the single amplitude $A=\pi/(\pi^2-2) = 0.3992 = 22.87^\circ$. This is illustrated by the surfaces of section in Fig.3. As A increases through A_{cr} it becomes unstable and there is a bifurcation, whose stable product is visible in Fig.3b. (Longer periodic orbits bouncing from inside, corresponding to slow motion of R with many swings of M between bounces, are all unstable, except for very small amplitudes $A \lesssim 4^\circ$.)

An obvious feature of Fig.3 are the large chaotic areas, showing that even this very simple model gives eternally irregular motion for a wide range of initial conditions. The chaos is however bounded above and below by invariant curves. These are associated with R

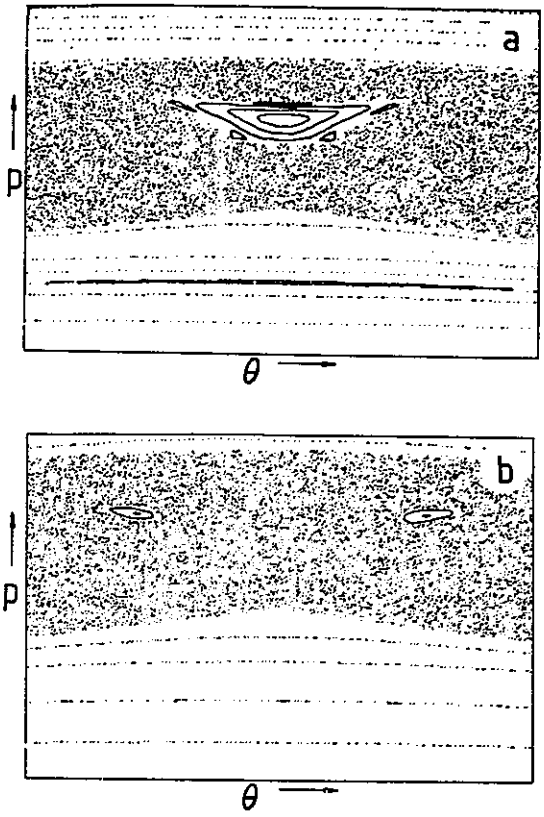

Fig.3. Surface of section mappings for the first model.
a) has $A=0.6(<A_{cr})$, $0<\theta<\pi$, $25<p<25$, and shows the stable fixed point (8) (2 bounce orbit) and associated KAM invariant curves and islands; b) has $A=\pi/2$ $(>A_{cr})$, $0<\theta<\pi$, $-30<p<30$, and shows that (8) is now unstable, but there is a new period-2 stable fixed point (4 bounce orbit). Both figures show large chaotic areas (each generated by a single orbit), and also adiabatic invariant curves for large enough $|p|$.

rotating so fast that M hardly moves between bounces, and suggests an adiabatic approximation in which the changes in ϕ are considered as continuous.

In obtaining the approximation, the starting-point is the Euler--Maclaurin type summation formula

$$\sum_{j=1}^{n}(F(2j)-F(2j-1)) \approx \frac{1}{2}(F(2n+1/2)-F(1/2)), \tag{11}$$

applied to the following exact relation, obtained from (3) and involving the bounce times t_n:

$$p_{2n} = p_o + 2\sum_{j=1}^{n}(d\phi(t_{2j})/dt - d\phi(t_{2j-1})/dt). \tag{12}$$

The result is an approximate conservation law relating even numbers of bounces:

$$p_{2n} - d\phi(t_{2n+1/2})/dt \approx p_o - d\phi(t_{1/2})/dt. \tag{13}$$

To convert this to a conserved phase-space function $K(\theta,p)$ on the surface of section, it is necessary to calculate the times $t_{2n+1/2}$ half-way between pairs of bounces 2n and 2n+1 separated by an integer time. After elementary geometry this gives

$$K(\theta,p) = p - 2\pi A \cos\{\frac{(\pi/2-\theta)2\pi}{p - 2\pi A}\} \qquad (14)$$

as the approximate constant of motion. Fig.4 shows those contours of K which connect $\theta=0$ and $\theta=\pi$. Comparison with Fig.3a shows qualitative agreement for all the invariant curves and quantitative agreement for large $|p|$ (where (14) ought to work). The approximation underestimates the size of the chaotic area.

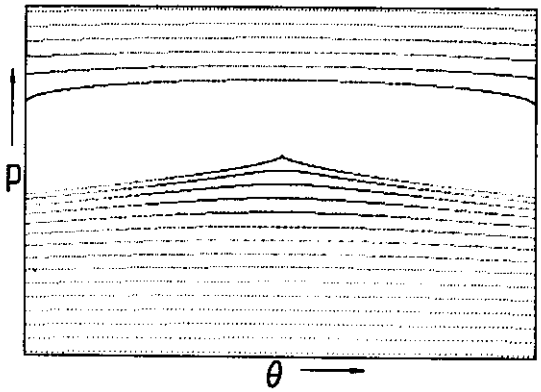

Fig.4 Contours of the approximate adiabatic invariant (14) for A=0.6, $0<\theta<\pi$, $-25<p<25$.

3 THE SECOND MODEL: INTRODUCING INDECISIVENESS

Because M has only finite strength, its repulsion does not cause a bounce at every encounter with R. We incorporate this feature of indecisiveness through a potential energy V depending on the angle between R and M and appearing in the rotator's Hamiltonian, which in units corresponding to a moment of inertia of unity is

$$H(\theta,p) = p^2/2 + V(\theta-\phi(t)). \qquad (15)$$

The repulsion is strongly localized near angles for which R passes M, so that the function V has the form shown in Fig.5. Each narrow potential barrier has height $Q^2/2$; for energies exceeding $Q^2/2$, the system passes 'over the barrier' and there is no bounce; for energies below $Q^2/2$, a bounce occurs. The parameter Q, whose value thus determines whether or not there will be a bounce, has a simple physical interpretaton: the relative angular velocity which must not be exceeded if an encounter is to result in a bounce. Motion therefore takes place according to eqs.(2-4) with the extra condition that t_B is a bounce time only if

$$\left|p(t_B)-d\phi(t_B)/dt\right| < Q. \qquad (16)$$

Some orbits are shown in Fig.6; which should be compared with Fig.2.

This second model therefore has two parameters: the magnet's strength Q and the swing amplitude A. The limit $Q\to\infty$ corresponds to the first model (guaranteed bouncing), and the limit $Q\to 0$ corresponds to the free rotator. For the bouncer, experiment (see section 4) indicates that $Q\sim 5$.

Bouncing occurs only if R passes M in a phase space bounce zone, for which according to (16), (1) and (2)

$$|p \pm 2\pi\sqrt{(A^2-\theta^2)}| < Q \qquad (17)$$

As Fig.7 shows, the form of these zones depends on $Q/2\pi A$. In

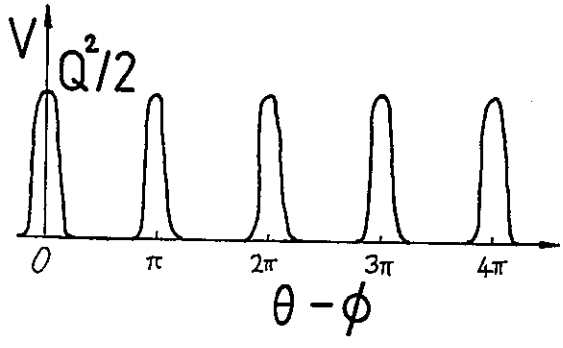

Fig.5. Angular potential energy V describing repulsion where R passes close to M. $-\partial V/\partial\theta$ gives the impulsive angular torque which may or may not result in a bounce, according to (16).

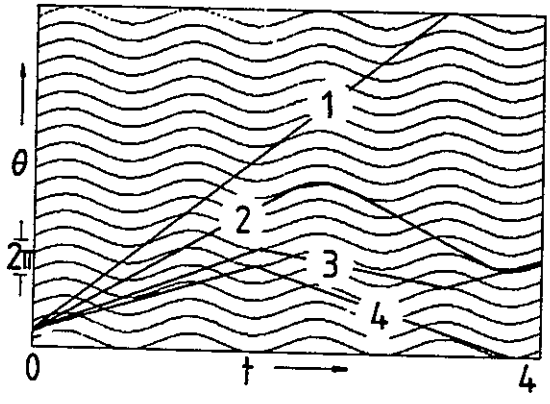

Fig.6. Orbits of the second model with A= $\pi/2$, Q=8, showing an orbit too fast to bounce (1) and three indecisively bouncing orbits (2-4). (Orbit 2 bounces several times in rapid succession). The sinusoids are $\phi(t) \bmod \pi$.

particular, if $Q<2\pi A$ there are bounce-free 'holes' near p=0, which which will play a crucial role later.

It is clear from (17) and Fig.7 that momenta $|p|>Q+2\pi A$ lie outside the bounce zones and so correspond to free rotation (with constant p) unaffected by M. For all momenta $|p|<Q+2\pi A$ there are some ranges of θ which do lie in a bounce zone, so all initial conditions in this range (except segments of the line p=0 for $Q<2\pi A$) will eventually bounce, albeit sometimes with many non-bouncing encounters corresponding to R passing M in one of the clear zones of Fig.7. If there are no closed orbits or adiabatic invariant curves (cf.Fig.3) lying entirely within a bounce zone, then the whole area $|p|<Q+2\pi A$ is expected to be covered chaotically by a single orbit. As Fig.8 confirms, this is indeed the case for realistic bouncer parameters, and begins to explain the observed irregular motion. (the stable period-2 fixed points in Fig.3b lie just outside the bounce zones, and leave this chaos unaffected.)

As Q increases, bounces become more likely, and there will be a

transition to the orbits of the first model. It would be interesting to explore this in detail (I have not done so).

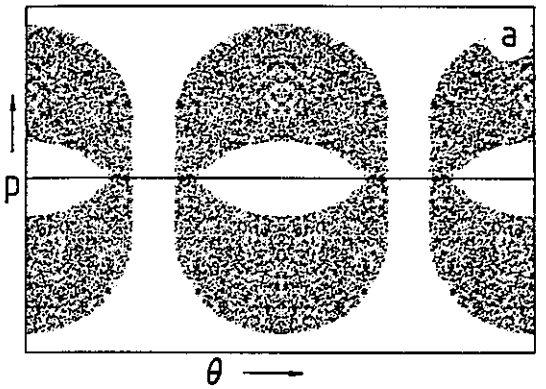

Fig.7 Phase-space bounce zones (shaded) for A=75° and a) Q=5 ($<2\pi A$), $0<\theta<2\pi$, $-15.9<p<15.9$; b) Q=10 ($>2\pi A$), $0<\theta<2\pi$ $-21.9<p<21.9$

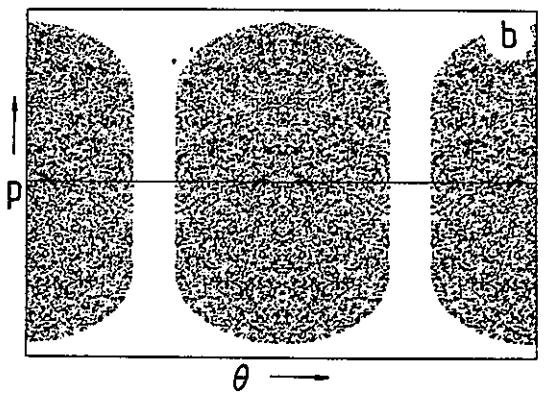

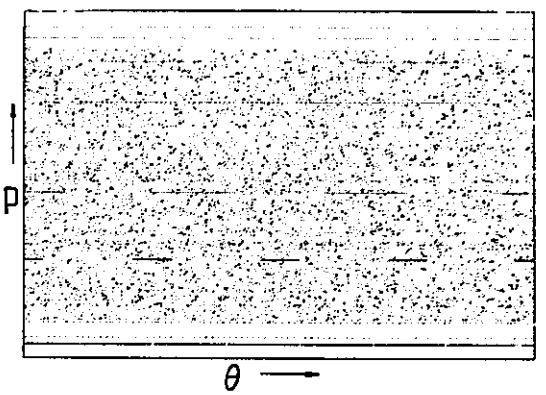

Fig.8 Surface of section mapping for the second model, with $A=\pi/2$, $Q=6$, $0<\theta<\pi$, $-20<p<20$. The region $|p| < Q+2\pi A=15.87$ is slowly covered by a single orbit, with chaotic wanderings separated by long sequences of bounce-free rotations (straight segments).

4. THE THIRD MODEL; INTRODUCING DISSIPATION

Between bounces, R slows down visibly, and if M is removed it comes

to rest in some fixed orientation in spite of the swinging of its axis A_1. This shows firstly that dissipation is important and secondly that air friction, inhibiting $d\theta/dt$, dominates bearing friction, which inhibits $d(\theta-\phi)/dt$. Ignoring all other sources of dissipation (e.g. eddy currents) we incorporate air friction by a linear torque, which when combined with the bounce torque from M gives the equations of this third model as

$$dp/dt = - Kp - \partial V(\theta-\phi(t))/\partial\theta \; ; \; d\theta/dt = p. \qquad (18)$$

K is a friction constant and constitutes a third parameter (the others are A and Q). (With this linear law the inertial forces arising from the transition to the accelerating frame with A_1 fixed do not contribute to the torque.)

To measure K for the bouncer, we disconnect the driving battery, remove M and use the following damped-rotator equation, which can be derived from (18) with V=0:

$$d\theta(t)/dt = d\theta(0)/dt - K(\theta(t)-\theta(0)). \qquad (19)$$

For $t\to\infty$ this gives $K = d\theta(0)/dt/[\theta(\;)-\theta(0)]$, easily measured by timing the first few rotations and counting the total number of turns before R comes to rest. The result is $K\sim 0.3$. To measure Q we replace M (battery still disconnected) and again use (19), this time counting the number of turns before the first bounce.

Between swings of the driver, i.e. for time steps of unity, the Jacobian determinant of the deviation matrix (5) is $\det M = \exp(-K)$, independently of any bounces that may have occurred. Therefore the mapping on the surface of section is area-contracting and all orbits must tend to an attracting set in the phase plane. In order to correspond to the apparently perpetual irregular motion of the bouncer, this would have to be a strange attractor [3,4], and it was confidently expected that computations with realistic parameters would reveal such a structure.

As Fig.9 shows, however, this confidence was misplaced: instead of being strange, the attractor is a fixed point. Different initial conditions, or different values of K, lead to different fixed points, but never a strange attractor.

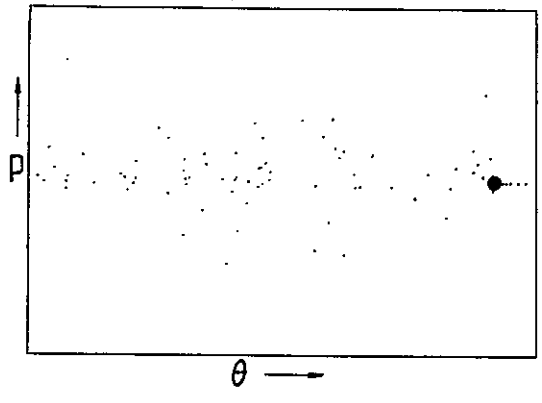

Fig.9 Surface of section mapping for the third model, with $A=\pi/2$, $Q=5$ and $K=0.3$, $0<\theta<\pi$, $-20<p<20$ showing attraction to a fixed point (filled circle). Note that $Q/2\pi A=0.51$

To understand this unexpected behaviour we note firstly that the parameters for which it occurs satisfy $Q<2\pi A$, and secondly that the attracting fixed points all have $p=0$, i.e. R at rest. Referring to Fig.7a we see that these points lie outside the phase-space bounce zones, and occupy segments of the θ axis which are invariant lines of

fixed points, stabilized by friction. The points therefore correspond to R near vertical (if $A \sim \pi/2$) with M passing too fast to cause a bounce.

To test this interpretation we eliminate the bounce-free zones by choosing $A > \pi/2$ and (increasing the strength of M so that $Q > 2\pi A$. Then computation always gives a strange attractor as Fig.10 illustrates in a striking way. But the parameters for which strange attractors occur are unrealistic, so these computations fail to explain the observed persistent irregularity of the bouncer.

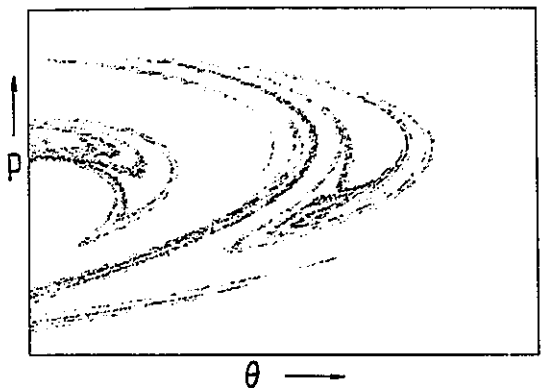

Fig.10 Surface of section mapping for the third model, with $A=2\pi/3, Q=\infty$ and $K=0.9$, $0<\theta<\pi$, $0<p<35$, showing the characteristic folded and multisheeted (fractal) structure of a strange attractor

5 THE FOURTH MODEL; INTRODUCING ILL-BALANCE

In the third model it was tacitly assumed that R was perfectly balanced and so could remain at rest in neutral equilibrium at any orientation, in particular those for which bouncing need not occur. The fact that the physical device does continue bouncing suggests that its operation depends on the inevitable symmetry-breaking associated with lack of balance of its rotator. Indeed, experiments with M removed show that R always slowly rotates so as to come to rest in a near-horizontal orientation. Therefore there is a weak gravitational torque turning R towards a bounce zone and because $A \sim \pi/2$ this destabilizes the line segments of attracting fixed points of the third model. We incorporate this effect by a θ-dependent potential $\lambda \sin\theta$, to give the equations of the fourth model as (cf.18)

$$dp/dt = -\lambda\cos\theta - Kp - \partial V(\theta - \phi(t))/\partial\theta \; ; \; d\theta/dt = p. \qquad (20)$$

Now there are four parameters: λ, A, Q and K. I estimated the value of λ as 0.015 but this is not critical. Any tendency to set horizontal (at $\theta = 3\pi/2$ if $\lambda > 0$), however slight, leads at last to perpetual irregular bouncing, as Fig.11 shows. For the realistic parameters of Fig.11a, the many-sheeted structure of the attractor is not very clear. Increasing K and λ (Fig.11b) emphasizes the sheets and gives an attractor with an unfamiliar 'fingered' appearance (see [5] for a faintly similar attractor, also occurring in a highly-damped driven impact system).

If, as is probable, the ill-balance of commercial bouncers arises from imperfections in manufacture, the stable orientations of their rotators can be expected to be distributed randomly over all angles. Only those machines for which the stable orientation lies in a bounce zone will display persistent irregularity. For $A=\pi/2, Q=5$ this is a restrictive condition: it selects orientations within 12.4° of

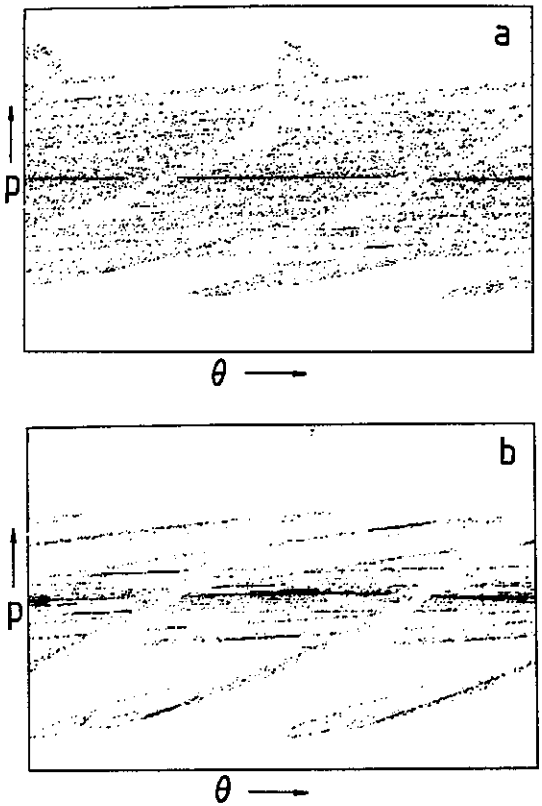

Fig.11 Surface of section mappings for the fourth model, with $A=\pi/2, Q=6$ and a) $K=0.3$, $\lambda=0.015$, $0<\theta<2\pi$, $-20<p<20$; b) $K=1$, $\lambda=0.2$, $0<\theta<2\pi$, $-12<p<12$. In (a), for which the parameters are realistic, the bounce-free segments of the axis $p=0$ are visible as horizontal lines along which the system slowly drifts before entering a bounce zone and being thrown onto one of the sheets of the attractor

horizontal, and leads to the prediction that most commercial machines will eventually stop bouncing and settle down with R swinging back and forth in a fixed orientation. This indeed happens (often only after many minutes); the manufacturers appear to regard it as inevitable, and in their operating instructions ascribe it to 'qualitative principle'! The theory can be easily tested with a horizontally-balanced (persistent) bouncer by unbalancing one of its balls with a light weight, to make it tend to hang vertically.

REFERENCES

1. A New English Dictionary on Historical Principles, vol.II (Oxford, 1893): Chaology (rare) "the history or description of the chaos"
2. G.Casati, J.Ford, F.Vivaldi and W.M.Visscher: Phys.Rev.Lett. 52, 1861-4(1984)
3. A.J.Lichtenberg and M.A.Lieberman: Regular and Stochastic Motion (Springer, New York 1983)
4. J.Guckenheimer and P.Holmes: Nonlinear Oscilations, Dynamical Systems and Bifurcations of Vector Fields (Springer, New York 1983)
5. S.W.Shaw: J.of Sound and Vib. in press 1984